

Surface wave isolation with the interferometric Green tensor

Kasper van Wijk*, Dylan Mikesell, Thomas Blum and Matt Haney, Boise State University
Alex Calvert, Ion Geophysical, now at Maersk Oil, Copenhagen

SUMMARY

Surface and body waves inherently coexist in seismic records. Usually, we are interested in the one, while the other is considered unwanted. To complicate things, body and surface waves often overlap in time and space. Hence, separation of these different wave modes is complicated, and remains an active topic of research. Here we use estimates of the Green tensor obtained via seismic interferometry to provide waveforms with isolated body and surface waves, allowing us to focus our further studies on one or the other. These ideas are illustrated with laboratory and numerical examples.

INTRODUCTION

The crosscorrelation of wavefields from sources of seismic energy provide an estimate of the Green function between receivers, as if there is a “virtual” source at one of the receiver locations. In principle, the sources should enclose the receiver locations, but in practice they seldom do. To recover an accurate Green function estimate with limited source coverage, one needs to sample the stationary phase points for coherent waves in the Green function. The virtual source location is the stationary phase point for all such events. However, this may not be the most informative case: typically we are interested in creating “virtual sources” where real sources are not present (Schuster et al., 2004; Bakulin et al., 2007).

Crosscorrelations of waveforms from sources away from the virtual source location may not provide the best body-wave Green function estimation. Even if we sample the stationary phase points of the different body waves well, cross-terms of correlations between the surface wave on one sensor and a body wave on the other sensor deteriorate the virtual shot record. For example, van Wijk (2006) essentially uses a receiver group (in the form of a large transducer recording surface) and then filtered out most of the remaining surface-wave energy before crosscorrelating to obtain an accurate body-wave Green function estimate.

However, in a 2D geometry the surface wave is accurately estimated with any in-line (far-offset) source. In essence, this forms the basis of the success of surface wave tomography with Green function estimates from the crosscorrelation of ambient seismic noise generated by the oceans (Shapiro and Campillo, 2004; Shapiro et al., 2005; Sabra et al., 2005). These results are obtained with estimates of the vertical component of the surface wave Green function.

Several groups have investigated surface-wave recovery by means of seismic interferometry and an adaptive process to remove these from the real data (Halliday et al., 2007; Xue et al., 2009), as alternatives to more conventional filtering techniques, such

as frequency-wavenumber and polarization filters on real data. We illustrate how the Green tensor can provide estimates dominated by the surface wave. This estimate can be used for adaptive surface wave suppression in the real data, or serve as “new” data for surface-wave dispersion inversion.

THEORY

The far-field approximation of elastic seismic interferometry is

$$G_{ij}(\mathbf{x}, \mathbf{x}', \omega) + G_{ij}^*(\mathbf{x}, \mathbf{x}', \omega) \approx \oint_S \frac{2G_{ki}^*(\mathbf{x}, \mathbf{x}'', \omega)G_{kj}(\mathbf{x}', \mathbf{x}'', \omega)}{\rho(\mathbf{x}'')c(\mathbf{x}'')} dS'', \quad (1)$$

where $G_{ij}(\mathbf{x}, \mathbf{x}', \omega)$ denotes the causal frequency domain Green tensor with component j at location \mathbf{x} from a point force source in direction i at \mathbf{x}' and $G_{ij}^*(\mathbf{x}, \mathbf{x}', \omega)$ denotes the complex conjugate Green tensor, which corresponds to the anti-causal time-domain Green tensor. $G_{ki}^*(\mathbf{x}, \mathbf{x}'', \omega)$ and $G_{kj}(\mathbf{x}', \mathbf{x}'', \omega)$ represent the Green tensor at \mathbf{x} and \mathbf{x}' due to a point force source in the k direction at \mathbf{x}'' located on the closed integration surface S around the receivers at \mathbf{x} and \mathbf{x}' . The density and velocity are presented by ρ and c , respectively.

In a 2D model, the causal Green tensor for the Rayleigh wave G_{ij}^R at the surface can be estimated from a single source at the surface:

$$G_{ij}^R(x, x', \omega) \propto G_{ki}^{R,*}(x, x'', \omega)G_{kj}^R(x', x'', \omega), \quad (2)$$

where the point source is in the k direction, and $x'' < x' < x$. In essence, this is what happens in ambient noise tomography. With the single source, body wave information is hard or impossible to decipher. In fact, the body-wave Green function in surface seismology is much harder to obtain, because with sensors at the surface the enclosing integration surface S of equation 1 is not feasible. This gives rise to spurious waves such as the virtual refraction (Mikesell et al., 2009), but also to opportunities to separate surface from body wave energy in the estimated Green function.

For surface sources and receivers in a vertically heterogeneous Earth, reciprocity and symmetry in the model determine that the Green tensor obeys (Aki and Richards, 1980):

$$\begin{aligned} G_{ij}(x, x', \omega) &= -G_{ji}(x', x, \omega) \quad \forall j \neq i, \\ G_{ij}(x, x', \omega) &= G_{ji}(x', x, \omega) \quad \forall j = i. \end{aligned} \quad (3)$$

Note that equation 2 did not have the limiting assumption of lateral homogeneity, but it may be that for small source-receiver distances, the lateral variation is negligible in practice.

Next, we will take advantage of how common surface-seismic acquisition geometries are inherently good at recovering the

interferometric surface wave isolation

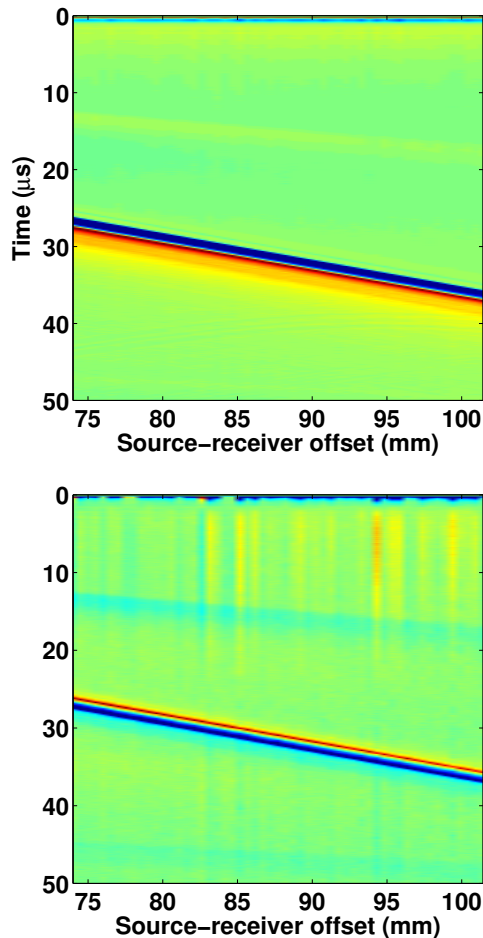


Figure 1: Vertical (top) and radial (bottom) components of a Rayleigh wave in homogeneous aluminum.

surface wave components, but relatively bad at estimating the body wave components in the Green tensor. This means the interferometrically obtained surface wave estimate follows equation 3, and the body wave estimate does not. First, let us show the former result.

A RAYLEIGH-WAVE LABORATORY EXAMPLE

We tested the idea of surface wave isolation with an ultrasonic Rayleigh wave in a homogeneous half-space of aluminum. Figure 1 shows the radial and vertical components of the Rayleigh wave recorded with a non-contacting laser receiver. The Rayleigh waves are generated with a powerful pulsed laser, creating thermoelastic expansion in the sample. For a complete description of the system, please visit (Blum et al., 2010).

Figure 2 contains G_{zx} , G_{xz} and G_{zz} in different combinations. In this case, we summed over 10 realizations by taking advantage of the lateral homogeneity of the sample. The results are that G_{zx} and G_{xz} are ± 90 degrees out of phase with G_{zz} , respectively. Taking advantage of this 180 degree phase between

each other, G_{zx} plus G_{xz} reduces (middle) and G_{zx} minus G_{xz} enhances (right) the surface wave with respect to the G_{zz} result. We still observe a small surface wave component in the middle panel, mainly because we have a small bias in our sensor that makes the vertical and radial components not exactly 90 degrees out of phase. Nevertheless, the suppression of the surface wave is significant. Next, let us show you how the body-wave estimates of the Green tensor from a similar acquisition geometry behave differently.

NUMERICAL EXAMPLE

In spectral-element simulations (Komatitsch and Tromp, 2002), vertical impact point-force sources at the surface range from 500 to 1050 m at 2 meter increments are recorded on 501 receivers, spaced every meter, ranging from 1050 to 1550 m (Figure 3). Each receiver records the vertical and horizontal component of the wavefield. The model has $Q_p=40$ and $Q_s=15$ and the wave speeds are defined in Figure 3. Figure 4 represents the vertical component of the wavefield from a vertical impact source at receiver 1. Coherent features are the linear direct P-wave and Rayleigh wave, the hyperbolic P-wave reflection (plus multiples), and a converted PS reflection, as well as a faint SS-wave. Figure 5 is the result of the crosscorrelation of the vertical component of the wavefield at receiver 1 with the vertical component of the wavefield at all receivers, summed over all sources located to the left of receiver 1. This estimate of G_{zz} is dominated by the surface wave, because of equation 2: each source contributes constructively to the Rayleigh wave retrieval between the virtual source and the receivers. Body-wave energy is the result of interference of primary reflection to the virtual source point with multiple reflection to the receivers (van Wijk, 2006).

The black line in Figure 6 is the trace at the receiver 200 m to the right of the virtual shot point location. The other two lines are the result of the summed crosscorrelation of the horizontal component of the wavefield at the virtual shot point with the vertical at the receiver (blue) and vice versa (red). These two are 180 degrees out of phase for the surface wave, but in this case in phase for the PP reflection at $t=0.2s$. This means that when we sum G_{zx} and G_{xz} , we highlight the PP reflection at the cost of the surface wave (Figure 7). In this example, the PP reflection is strongest at the intermediate offsets, because it is for these offsets that PP energy is significant on both the vertical and the horizontal components of the wavefield. Observe that if our Green function retrieval procedure would have been accurate for body waves reflections (as it is for direct waves), $G_{zx}+G_{xz} = 0$, for all wave modes, by virtue of equation 3. It is the limited source aperture that gives rise to a strong PP reflection in $G_{zx}+G_{xz}$.

Alternatively, the difference $G_{zx}-G_{xz}$ results in a cleaner surface wave representation (Figure 8) than in the vertical component correlations of Figure 5. This result can be the starting point for adaptive surface wave removal from active seismic data. Alternatively, this strong surface wave could be directly used for subsurface parameter estimation. The ocean noise correlation technique added a new dimension to passive seis-

interferometric surface wave isolation

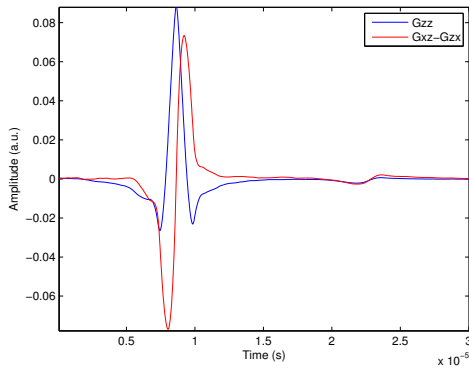
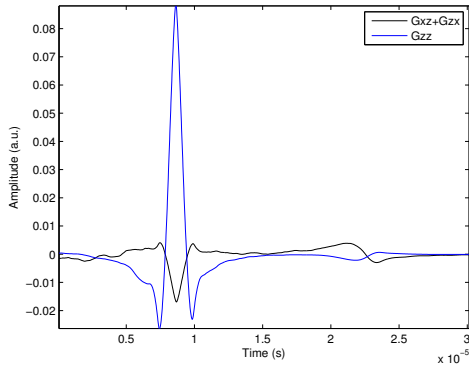
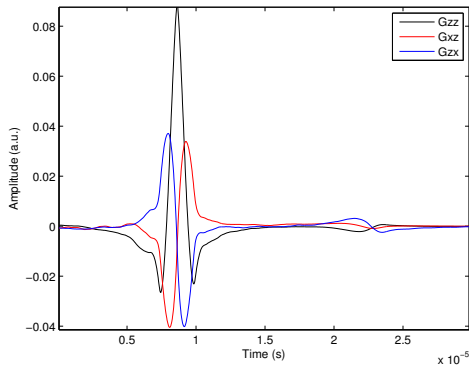


Figure 2: G_{zx} and G_{xz} (top), G_{xz} plus G_{zx} (middle) and G_{zx} minus G_{xz} (bottom).

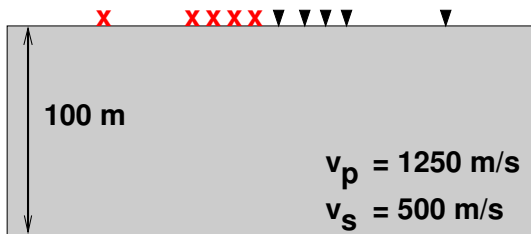


Figure 3: Parameters of a two-dimensional numerical model with attenuation.

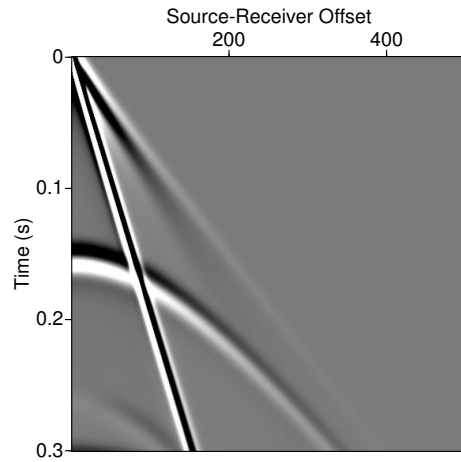


Figure 4: Vertical component of the wavefield from a vertical force source.

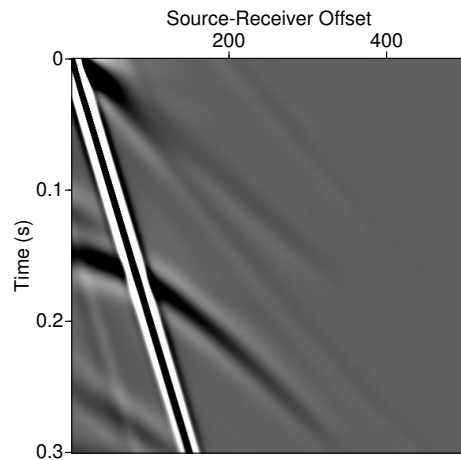


Figure 5: Estimate of the virtual shot record for the vertical component from crosscorrelations of the vertical components summed over many sources.

interferometric surface wave isolation

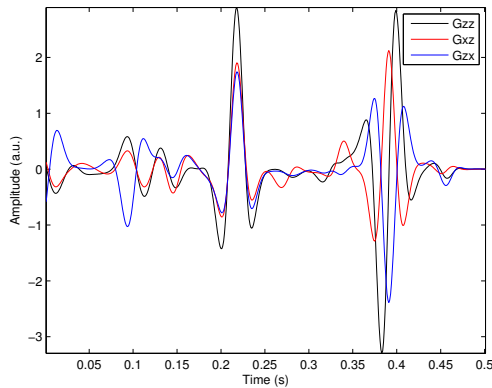


Figure 6: Different components of the estimated Green function with the source 200 m to the left of the receiver (left). The direct P-wave arrives at $t=0.1s$, the reflected (PP) wave at $t=0.2s$ and the surface wave at $t=0.4s$.

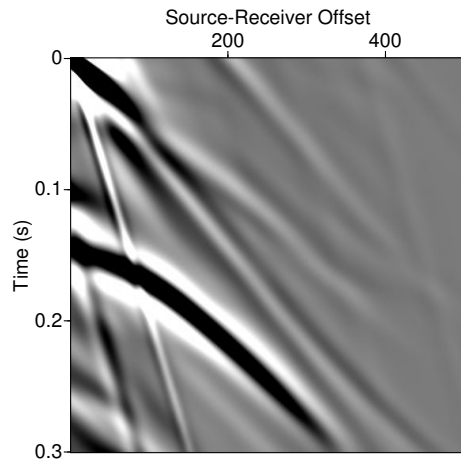


Figure 7: $Gzx+Gxz$ for surface seismics in a slab highlights wave modes other than surface waves. In this case, the PP reflections is particularly dominant.

mology (e.g., Campillo and Paul, 2003; Shapiro and Campillo, 2004; Shapiro et al., 2005; Sabra et al., 2005). These Green function estimates are dominated by surface waves, whose dispersion is inverted for subsurface information. $Gzx+Gxz$ suppresses the surface waves, and may show other wave types, such as scattered surface waves, and possibly refracted and reflected waves.

Whether subtracting or highlighting the surface waves, the method is a point operation. There are no problems with spatial aliasing or other array-related issues, hence station separation can be large. However, we are assuming lateral homogeneity, which may not be practical in certain cases, or only locally true.

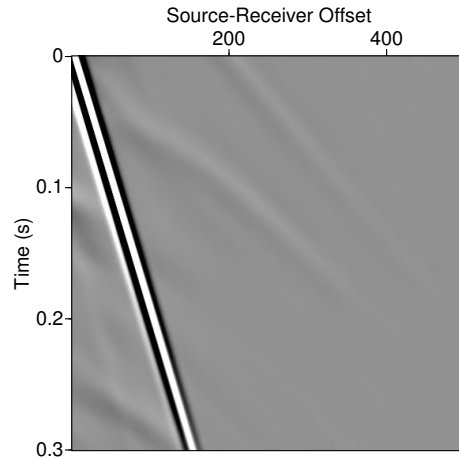


Figure 8: $Gzx-Gxz$ leads to optimal surface-wave retrieval in this geometry. In a multi-layered medium, one could use its dispersive properties to invert for subsurface structure.

FUTURE WORK

Soon we hope to remove surface waves in exploration seismic data, but also in the interferometrically obtained Green function in regional seismic networks, such as the Transportable Array. While current correlations are dominated by surface waves, there may be other coherent events to be discovered. Alternatively, we anticipate to invert isolated dispersive surface waves for subsurface parameters.

CONCLUSION

In multi-component surface seismology in a horizontally layered Earth, summing (interferometrically obtained) Gzx and Gxz contains little or no surface-wave energy, potentially boosting other wave modes with signal on the vertical and horizontal components. In ocean noise interferometry, we can search for scattered surface waves and body waves, after the surface wave suppression. Alternatively, the difference between Gzx and Gxz provides an enhanced surface wave. This can potentially be used for adaptive surface wave removal in exploration seismology, or cleaner surface wave inversion from its dispersive properties.

ACKNOWLEDGMENTS

We thank Ludmila Adam, Roel Snieder, and Alison Malcolm for their stimulating discussions and suggestions.

EDITED REFERENCES

Note: This reference list is a copy-edited version of the reference list submitted by the author. Reference lists for the 2010 SEG Technical Program Expanded Abstracts have been copy edited so that references provided with the online metadata for each paper will achieve a high degree of linking to cited sources that appear on the Web.

REFERENCES

- Aki, K., and P. G. Richards, 1980, Quantitative seismology: theory and practice: Freeman.
- Blum, T., K. van Wijk, B. Pouet, and A. Wartelle, 2010, Multi-component wavefield characterization with a novel scanning laser interferometer: *Review of Scientific Instruments*, **81**, no. 1, 1-4
- Campillo, M., and A. Paul, 2003, Long-range correlations in the diffuse seismic coda: *Science*, **299**, no. 5606, 547–549, [doi:10.1126/science.1078551](https://doi.org/10.1126/science.1078551). [PubMed](#)
- Halliday, D. F., A. Curtis, J. O. A. Robertsson, and D.-J. van Manen, 2007, Interferometric surface-wave isolation and removal: *Geophysics*, **72**, no. 5, A69–A73, [doi:10.1190/1.2761967](https://doi.org/10.1190/1.2761967).
- Komatitsch, D., and J. Tromp, 2002, Spectral-element simulations of global seismic wave propagation—I. Validation: *Geophysical Journal International*, **149**, no. 2, 390–412, [doi:10.1046/j.1365-246X.2002.01653.x](https://doi.org/10.1046/j.1365-246X.2002.01653.x).
- Lopez, 2007, Virtual shear source makes shear waves with air guns: *Geophysics*, **72**, A7–A11.
- Mikesell, D., K. van Wijk, A. Calvert, and M. Haney, 2009, The virtual refraction: Useful spurious energy in seismic interferometry: *Geophysics*, **74**, no. 3, A13–A17, [doi:10.1190/1.3095659](https://doi.org/10.1190/1.3095659).
- Sabra, K. G., P. Gerstoft, P. Roux, W. A. Kuperman, and M. C. Fehler, 2005, Surface wave tomography from microseisms in Southern California : *Geophysical Research Letters*, **32**, no. 14, L14311–L14314, [doi:10.1029/2005GL023155](https://doi.org/10.1029/2005GL023155).
- Schuster, G. T., J. Yu, J. Sheng, and J. Rickett, 2004, Interferometric/daylight seismic imaging: *Geophysical Journal International*, **157**, no. 2, 838–852, [doi:10.1111/j.1365-246X.2004.02251.x](https://doi.org/10.1111/j.1365-246X.2004.02251.x).
- Shapiro, N. M., and M. Campillo, 2004, Emergence of broad-band Rayleigh waves from correlations of the ambient seismic noise: *Geophysical Research Letters*, **31**, no. 7, L07614, [doi:10.1029/2004GL019491](https://doi.org/10.1029/2004GL019491).
- Shapiro, N. M., M. Campillo, L. Stehly, and M. H. Ritzwoller, 2005, High-resolution surface-wave tomography from ambient seismic noise: *Science*, **307**, no. 5715, 1615–1618, [doi:10.1126/science.1108339](https://doi.org/10.1126/science.1108339). [PubMed](#)
- van Wijk, K., 2006, On estimating the impulse response between receivers in a controlled ultrasonic experiment: *Geophysics*, **71**, no. 4, SI79–SI84, [doi:10.1190/1.2215360](https://doi.org/10.1190/1.2215360).
- Xue, Y., S. Dong, and G. T. Schuster, 2009, Interferometric prediction and subtraction of surface waves with a nonlinear local filter: *Geophysics*, **74**, no. 1, SI1–SI8, [doi:10.1190/1.3008543](https://doi.org/10.1190/1.3008543).